# CEBAF Program Advisory Committee Eight Cover Sheet

This proposal must be received by close of business on Thursday, April 14, 1994 at:

CEBAF
User Liaison Office, Mail Stop 12 B
12000 Jefferson Avenue
Newport News, VA 23606

**Proposal Title**

Measurement of the Neutron ($^3$He) spin structure function at low $Q^2$; a connection between the BJ and DHG sum rules

**Contact Person**


Name: Z. E. MEZIANI.
Institution: TEMPLE UNIVERSITY
Address: Department of Physics, BARTON HALL
Address: 13th & Norris St.
City, State ZIP/Country: PHILADELPHIA
Phone: (215) 204 5971 FAX: (215) 204 5652
E-Mail → Internet: MEZIANI@VM.TEMPLE.EDU


Experimental Hall: A
Total Days Requested for Approval: 34
Minimum and Maximum Beam Energies (GeV): 1.6 GeV 4 GeV
Minimum and Maximum Beam Currents (μAmps): 1 μA 15 μA

**CEBAF Use Only**

Receipt Date: 3/14/94

By:

# Measurement of the Neutron ($^3$He) Spin Structure Function at Low $Q^2$; a connection between the Bjorken and Drell-Hearn-Gerasimov Sum Rules

B. Filippone, W. Korsch, A. Lung, R. Mckeown, M. Pitt

*California Institute of Technology, Pasadena, California 91125*

P.M. Rutt

*University of Georgia and Rutgers University, NJ 08855*

B. Anderson, G.G. Petratos, J. Watson

*Kent State University, Kent, OH 44242*

P. Bogorad, G.D. Cates, K.F. Kumar, H. Middleton

*Princeton University, Princeton, NJ 08544*

C. Glasshausser, R. Gilman, Ed. Brash, L. Bimbot, R.D. Ransome

*Rutgers University, Rutgers, NJ 08855*

R. Holmes, X. Wang, J. McCracken, P.A. Souder

*Syracuse University, Syracuse, NY 13122*

D. Kawall

*Stanford University, Stanford, California 94305*

L. Auerbach, J. Margulies, J. Martoff, Z.-E. Meziani

*Temple University, Philadelphia, PA 19122*

Spokespersons: G. Cates, Z.-E. Meziani

## ABSTRACT

We propose to determine the virtual photon-neutron longitudinal asymmetry $A_1^n(\nu, Q^2)$ and the spin-dependent structure function $g_1^n$ across the resonance and inelastic region by measuring the reaction $^3\vec{H}e(\vec{e}, e')$ over a wide range of four-momentum transfer $Q^2$ and energy transfer $\nu$. Using the CEBAF logitudinally polarized electron beam combined with a high pressure polarized $^3$He target, we propose to measure the inclusive spin dependent cross section with beam and target helicity parallel and antiparallel at four incident beam energies (E = 1.6 GeV, 2.4 GeV, 3.2 and 4. GeV) and three scattering angles 15°, 25°and 35°. The Hall A HRS spectrometers in their configuration for electron detection shall be used as two independent single arm spectrometers to double the solid angle and allow flexibility in the data taking at different angles.

In the limit $Q^2 \rightarrow 0$ the Bjorken sum is connected to the difference between the proton and neutron magnetic moments via the difference $I_p^{DHG} - I_n^{DHG}$ where $I^{DHG}$ is the Drell-Hearn Gerassimov sum rule. In this measurement we shall first study the $Q^2$ evolution of the neutron extended DHG sum rule. Furthermore together with the measurement proposed in Hall B (PR-91-023) and that of SLAC (E-143; E=9.7 GeV, $\theta = 4.5°$) this experiment allows the investigation of the $Q^2$ evolution of the Bjorken sum rule $I^{Bj}(Q^2)$ from $Q^2 \geq 2(GeV)^2$ down to $Q^2 \geq 0.15(GeV)^2$ and therefore will help clarify the structure of QCD rather than PQCD.

We estimate that 4 days of set up followed by a month of running will be sufficient to provide precision data which should discriminate between different evolution models of the extended DHG sum rule on the neutron. These measurements are complementary to those of Hall B experiment (E-93-009), and when combined with the proton measurement of Hall B and the SLAC E-143 measurement, the proposed CEBAF experiments will allow a first study of the low $Q^2$ evolution of the Bjorken sum rule.

# 1. Introduction and Motivation

The Bjorken sum rule, a fundamental sum rule of QCD has been recently the focus of several experimental investigations [1-3] . This sum rule was derived in the Bjorken limit where $Q^2 \to \infty$ and $\nu \to \infty$ but finite Bjorken variable $x = Q^2/2M\nu$.

The $Q^2$ range of the present data (Figure 1) of the nucleon spin structure function makes the investigation of its $Q^2$ evolution from infinity to finite momentum transfer ($Q^2 \geq 1$ GeV$^2$) rather important. At finite $Q^2$ higher order corrections must be understood to permit an experimental test of the sum rule. The corrections are cast into two categories; first those known as higher order PQCD corrections which are proportional to powers of $\alpha_s(Q^2)$ (the strong coupling constant). These corrections are dominant in the region $Q^2 \geq 5$ GeV$^2$ but have been accurately estimated [4]. Second those known as higher twist corrections [5] proportional to powers of $1/Q^2$ and consequently would govern the low $Q^2$ behavior of the nucleon spin structure function $g_1$, and ultimately the sum rule.

A study of the corrections at reasonably low $Q^2$ is directly related to understanding the structure of QCD rather than PQCD. These corrections have been recently the focus of an intensive debate given their direct impact on the Bjorken sum rule and on the extraction of the nucleon spin content. Several authors [7,8,9] are looking into the evolution of the Bjorken sum rule at values of $Q^2$ lower than 1 GeV. The $Q^2$ evolution of the first moments of the spin structure functions $g_1^n$ and $g_1^p$ are also investigated using the well known result of the Drell-Hearn-Gerassimov (DHG) sum rule [10]. It was recently pointed out [11] that in the real photon limit, the first moment of the spin structure function of the nucleon $g_1(x, Q^2)$ is related to the anomalous magnetic moment of the nucleon and therefore by exploring the $Q^2$ variation between this low energy limit and the well known scaling limit one can gain insight into the structure of QCD ( i.e. for example the operator product expansion analysis in QCD.)

At present an important experimental program has been launched at CERN, HERA, SLAC to investigate in the scaling region polarized deep-inelastic spin structure of the nucleon using polarized deuteron and $^3$He targets as polarized neutron targets. The goal is to look at the PQCD region (high $Q^2$ and deep-inelastic) and test the Bjorken sum rule to the highest precision. At the real photon limit ($Q^2 = 0$) the experimental results on the DHG sum rule are still puzzling. The disagreement between the experimental estimate through the analysis of photopion data and the predicted value from the DHG sum rule led to a new set of challenging total photoabsorption experiments with real photon beams around the world.

Recently several theoretical groups [12,13] have been investigating the $Q^2$ evolution of the extended DHG sum rule. The results of different groups show significant differences in the $Q^2$ evolution, which can be tested experimentaly. It has been also argued [14] that the $Q^2$ dependence of DHG is naturally described by using the Schwinger sum rules and the contribution of the $g_2$ spin structure function. This structure function, believed to be small at large $Q^2$, is totally unknown at low $Q^2$. It is the goal of this proposed experiment in a first stage to provide precision data on the spin structure function of the neutron $g_1^n$, connecting the deep inelastic region to the very low momentum transfer region.

We believe that CEBAF can significantly contribute to the exploration of the $Q^2$ evolution of the nucleon spin dependent structure functions and bridge the gap between these two physics regions allowing a better handle on the non perturbative aspects of QCD.

## 2. Asymmetries and Sum Rules

In deep-inelastic scattering, the measured longitudinal asymmetry $A^{\parallel}$ can be determined experimentally by measuring the ratio of the difference to the sum of cross sections for polarized electrons on polarized nucleons between states where the spins are parallel and antiparallel [15,16],

$$A^{\parallel} = \frac{\sigma^{\uparrow\downarrow} - \sigma^{\uparrow\uparrow}}{\sigma^{\uparrow\downarrow} + \sigma^{\uparrow\uparrow}} = \frac{1-\epsilon}{(1-\epsilon R)\ W_1(Q^2,\nu)} \left[M(E+E'\cos\theta)\ G_1(Q^2,\nu) - Q^2 G_2(Q^2,\nu)\right] . \quad (2.1)$$

Here $\sigma^{\uparrow\uparrow}$ ($\sigma^{\downarrow\uparrow}$) is the inclusive $d^2\sigma^{\uparrow\uparrow}/d\Omega d\nu$ ($d^2\sigma^{\downarrow\uparrow}/d\Omega d\nu$) differential scattering cross section for longitudinal target spins parallel (antiparallel) to the incident electron spins. A corresponding relationship exists for scattering of longitudinally polarized electrons off a transversely polarized target where a transverse asymmetry is defined [16]:

$$A^{\perp} = \frac{\sigma^{\downarrow\leftarrow} - \sigma^{\uparrow\leftarrow}}{\sigma^{\downarrow\leftarrow} + \sigma^{\uparrow\leftarrow}} = \frac{(1-\epsilon)E'}{(1-\epsilon R)\ W_1(Q^2,\nu)} \left[(MG_1(Q^2,\nu) + 2EG_2(Q^2,\nu))\ \cos\theta\right] , \quad (2.2)$$

where

$$R = \frac{W_2}{W_1}\left(1+\frac{\nu^2}{Q^2}\right) - 1 ; \qquad \epsilon = \left[1 + 2\left(1+\frac{\nu^2}{Q^2}\right)\ \tan^2\frac{\theta}{2}\right]^{-1} . \quad (2.3)$$

Here $\sigma^{\downarrow\leftarrow}(\sigma^{\uparrow\leftarrow})$ is the inclusive scattering cross section for beam-spin antiparallel (parallel) to the beam momentum, and for target-spin direction transverse to the beam momentum and towards the direction of the scattered electron. In all cases, $G_1$ and $G_2$ are the spin-dependent structure functions, whereas $W_1$ and $W_2$ are the spin-averaged structure functions; $R$ is the ratio of longitudinal-to-transverse virtual-photoabsorption cross sections; $\epsilon$ is the virtual photon polarization; $M$ is the mass of the nucleon; $Q^2$ is the square of the four-momentum of the virtual photon; $E$ is the incident electron energy; $E'$ is the scattered electron energy; $\nu = (E - E')$ is the electron energy loss; and $\theta$ is the electron scattering angle.

The system of Eqs. (2.1) and (2.2) allows for the separate determination of $G_1$ and $G_2$, knowing $W_2$ and $W_1$. In the scaling limit ($\nu$ and $Q^2$ large), these structure functions are predicted to depend only on the Bjorken variable $x = Q^2/2M\nu$, yielding

$$\begin{aligned} MW_1(\nu, Q^2) &\to F_1(x) , & \nu W_2(\nu, Q^2) &\to F_2(x) , \\ M^2\nu G_1(\nu, Q^2) &\to g_1(x) , & M\nu^2 G_2(\nu, Q^2) &\to g_2(x) . \end{aligned} \tag{2.4}$$

The experimental asymmetries $A^{\parallel}$ and $A^{\perp}$ are related to the virtual photon-nucleon longitudinal and transverse asymmetries, $A_1$ and $A_2$ respectively, via

$$\begin{aligned} A^{\parallel} &= D(A_1 + \eta A_2) , & A^{\perp} &= d(A_2 - \zeta A_1) , \\ D &= (1 - E'\epsilon/E)/(1 + \epsilon R) , & d &= D\sqrt{2\epsilon/(1+\epsilon)} \\ \eta &= \epsilon\sqrt{Q^2}/(E - E'\epsilon) , & \zeta &= \eta(1+\epsilon)/2\epsilon . \end{aligned} \tag{2.5}$$

The neutron spin structure function is extracted in the finite $Q^2$ region following the relation

$$g_1^n = \left[ A_1^n F_1^n + A_2^n F_1^n \left( \frac{2Mx}{\nu} \right)^{1/2} \right] \Bigg/ \left( 1 + \frac{2Mx}{\nu} \right) , \tag{2.6}$$

where $F_1^n$ is the spin averaged structure function of the neutron. Within the QPM interpretation, $F_1^n(x)$ and $g_1^n(x)$ are related to the momentum distribution of the constituents as

$$F_1(x) = \frac{1}{2} \sum_{i=1}^{f} z_i^2 \left[ q_i^{\uparrow}(x) + q_i^{\downarrow}(x) \right] , \qquad g_1(x) = \frac{1}{2} \sum_{i=1}^{f} z_i^2 \left[ q_f^{\uparrow}(x) - q_f^{\downarrow}(x) \right] , \tag{2.7}$$

where $i$ runs over the number of flavors, $z_i$ are the quark fractional charges, and $q_i^{\uparrow}$, $(q^{\downarrow})_i$ are the quark plus antiquark momentum distributions for quark and antiquarks spins parallel (antiparallel) to the nucleon spin.

The Bjorken sum rule is expressed to first order in $\alpha_s$ as the difference between the proton and the neutron spin structure function $g_1(x, Q^2)$ integrals.

$$I^{Bj} = I^p - I^n = \int_0^1 g_1^p(x, Q^2) - g_1^n(x, Q^2)\, dx = \frac{1}{12}\frac{g_A}{g_V}\left[1 - \frac{\alpha_s(Q^2)}{\pi}\right] . \qquad (2.8)$$

This sum rule is insensitive to the details of nucleon structure but depends solely on quark current algebra and isospin symmetry. Higher order PQCD [4], as well as higher twist [7] corrections, although not included in Eq. (2.8), are important in the analysis of the Bjorken sum rule and must be considered at low $Q^2$.

In connection with real photon experiments the quantities $A_1$ and $A_2$ can also be expressed in terms of the transverse virtual photo-absorption cross sections with a total helicity 1/2 and 3/2:

$$A_1 = \frac{\sigma_T^{1/2} - \sigma_T^{3/2}}{\sigma_T^{1/2} + \sigma_T^{3/2}}$$

and

$$A_2 = \frac{\sigma_{TL}}{\sigma_T^{1/2} + \sigma_T^{3/2}}$$

where $\sigma_{TL}$ is the longitudinal-transverse interference virtual photo-absorption cross section.

The DHG sum rule is expressed using the same cross sections but with real photons (at $Q^2 = 0$):

$$I^{DHG} = \int_{\nu_{thr}}^{\infty} [\sigma_N^{1/2} - \sigma_N^{3/2}]\frac{d\nu}{\nu} = -\frac{2\pi^2\alpha}{M^2}\kappa_N^2$$

where $\kappa_N$ is the anomalous magnetic moment and $M$ th mass of the nucleon. The DHG sum rule is extended to the virtual photon region by writing;

$$I^{DHG}(Q^2) = \int_{\nu_{thr}}^{\infty} [\sigma_T^{1/2} - \sigma_T^{3/2}]\frac{d\nu}{\nu} = -\frac{2\pi^2\alpha}{M^2}\kappa_N^2.$$

Equivalently it can be expressed using the quantity $A_1$,

$$I^{DHG}(Q^2) = \int_{\nu_{thr}}^{\infty} 2\sigma_T(Q^2,\nu)A_1(Q^2,\nu)\frac{d\nu}{\nu} = -\frac{2\pi^2\alpha}{M^2}\kappa_N^2$$

This extended DHG sum rule can then be connected to the Bjorken sum rule expression at any $Q^2$ by taking the difference between the proton and the neutron. In the case of real photons we have $I_p^{DHG} = -204.5\mu b$, $I_n^{DHG} = -232.8\mu b$ and $I_{p-n}^{DHG} = 28.3\mu b$. This latter value, (equivalent to forming the Bjorken sum at $Q^2 = 0$) is predicted to be positive. This is in disagreeent with analyses [17,18,19] of the present real photon measurement data where the results have the opposite sign and range between $-78\mu b$ and $-109\mu b$.

## 3. The Experimental Procedure

We propose to use a high pressure polarized $^3$He target and the longitudinally polarized electron beam in Hall A at CEBAF to measure the helicity dependent inclusive cross sections with beam and target spins parallel and antiparallel. We will also measure the cross sections with and target spins parpendicular to minimize the systematic error due to $A_2$ in extracting $g_1$. The measurement will be performed at four different energies ($E_i$ = 4.0, 3.2 , 2.4 and 1.6 GeV) and three different scattering angles (15°, 25°and 35°). The measurement will cover the resonance region at low $Q^2$ and high $Q^2$ and extend the E-142 measurement in the inelastic region $W^2 \geq 4$ at low $Q^2$ (Figure 2).

### 3.1 Polarized beam

Given the technical developments presently achieved with strained GaAs cathodes at SLAC (E-143) and other places we hope that high polarizations ( 80%) will be as well possible at CEBAF. Although the currents used in experiment E-143 were small (few tens of nanoamps), the newly approved experiment at 50 GeV (E-154) is planning to use similar value of polarization with few microamps average beam currents. SLAC is confident to reach

large electron beam polarizations with high currents. We shall assume in this proposal that the achievable beam polarization at CEBAF is 80% [20]. We are planning to use a beam current of 15 $\mu A$ due to depolarization effects on the $^3$He target, this would put us in a favorable situation given the ultimate goal of high currents and high polarization pursued at CEBAF. We believe that we can still do a significant measurement even if the polarization of the beam is about 50 to 60% since we are not limited by the statistical error.

### 3.2 The Polarized $^3$He Target

The polarized target will be based on the principle of spin exchange between optically pumped alkali-metal vapor and noble-gas nuclei [23,24,25]. The design will be similar in many ways to that used in E-142, an experiment at SLAC to measure the spin dependent structure function of the neutron [2]. A central feature of the target will be sealed glass target cells, which will contain a $^3$He pressure of about 10 atmospheres. As indicated in Fig. 3, the cells will have two chambers, an upper chamber in which the spin exchange takes place, and a lower chamber, through which the eletron beam will pass. In order to maintain the appropriate number density of alkali-metal (which will probably be Rb) the upper chamber will be kept at a temperature of 170–200 $^\circ C$ using an oven constructed of the high temperature plastic Torlon. With a density of $2.5 \times 10^{20}$ atoms/cm$^3$, and a lower cell length of 40 cm. the target thickness will be $1.0 \times 10^{22}$atoms/cm$^2$.

We describe below in greater detail some features of the target.

#### 3.2.1 Operating Principles

The time evolution of the $^3$He polarization can be calculated from a simple analysis of spin-exchange and $^3$He nuclear relaxation rates [21]. Assuming the $^3$He polarization $P_{^3He} = 0$ at $t = 0$,

$$P_{^3\mathrm{He}}(t) = \langle P_{\mathrm{Rb}} \rangle \left( \frac{\gamma_{\mathrm{SE}}}{\gamma_{\mathrm{SE}} + \Gamma_R} \right) \left( 1 - e^{-(\gamma_{\mathrm{SE}} + \Gamma_R)t} \right) \tag{3.1}$$

where $\gamma_{\mathrm{SE}}$ is the spin-exchange rate per $^3$He atom between the Rb and $^3$He, $\Gamma_R$ is the relaxation rate of the $^3$He nuclear polarization through all channels other than spin exchange with Rb, and $\langle P_{\mathrm{Rb}} \rangle$ is the average polarization of a Rb atom. Likewise, if the optical pumping is turned off at $t = 0$ with $\mathrm{P}_{^3\mathrm{He}} = \mathrm{P}_0$, the $^3$He nuclear polarization will decay according to

$$\mathrm{P}_{^3\mathrm{He}}(\mathrm{t}) = \mathrm{P}_0 e^{-(\gamma_{\mathrm{SE}} + \Gamma_{\mathrm{R}})\mathrm{t}} \tag{3.2}$$

The spin exchange rate $\gamma_{\mathrm{SE}}$ is defined by

$$\gamma_{\mathrm{SE}} \equiv \langle \sigma_{\mathrm{SE}}\, v \rangle [\mathrm{Rb}]_{\mathrm{A}} \tag{3.3}$$

where, $\langle \sigma_{\mathrm{SE}}\, v \rangle = 1.2 \times 10^{-19}$ cm$^3$/sec is the velocity-averaged spin-exchange cross section for Rb–$^3$He collisions [21,26,27] and $[\mathrm{Rb}]_{\mathrm{A}}$ is the average Rb number density seen by a $^3$He atom. Our target will be designed to operate with $1/\gamma_{\mathrm{SE}} = 8$ hours.

From equation (3.1) it is clear that there are two things that we can do to get the best possible $^3$He polarization — maximize $\gamma_{\mathrm{SE}}$ and minimize $\Gamma_{\mathrm{R}}$. But from equation (3.3) it is also clear that maximizing $\gamma_{\mathrm{SE}}$ means increasing the alkali-metal number density, which in turn means more laser power. The number of photons needed per second must compensate for the spin relaxation of Rb spins. In order to achieve $1/\gamma_{\mathrm{SE}} = 8$ hours, we will require about 24 Watts of usable laser light at a wavelength of 795 nm. We will say more about the source of laser light below.

The rate at which polarization is lost, which is characterized by $\Gamma_{\mathrm{R}}$, will have four principle contributions. An average electron beam current of about 15 $\mu$A will result in a

depolarization rate of $\Gamma_{beam} = 1/30$ hours [30]. Judging from experience at SLAC, we can produce target cells with an intrinsic rate of $\Gamma_{cell} = 1/50$ hours. This has two contributions, relaxation in that occurs during collisions of $^3$He atoms due to dipole-dipole interactions [28], and relaxation that is presumably due largely to the interaction of the $^3$He atoms with the walls. Finally, relaxation due to magnetic field inhomogeneities can probably be held to about $\Gamma_{\nabla B} = 1/100$ hours. Collectively, under operating conditions, we would thus expect

$$\Gamma = \Gamma_{beam} + \Gamma_{cell} + \Gamma_{\nabla B} = 1/30\text{hours} + 1/50\text{hours} + 1/100\text{hours} = 1/16\text{hours}. \quad (3.4)$$

Thus, according to (3.4), the target polarization cannot be expected to exceed

$$P_{max} = \frac{\gamma_{SE}}{\gamma_{SE} + \Gamma} = 0.66$$

Realistically, we will not achieve a Rb polarization of 100% in the pumping chamber, which will reduce the polarization to about 45–50%.

### 3.2.2 Target Cells

The construction and filling of the target cells must be accomplished with great care if $1/\Gamma_{cell}$ is to be in excess of 50 hours. We plan to use the "Princeton Prescription", which resulted, among the cells that were tested, in lifetimes that were always better than 30hours, and in about 60% of the cells, better than 50 hours. The following precautions will be taken:

- Cells will be constructed from aluminosilicate glass.
- All tubing will be "resized". This is a process in which the diameter of the tubing is enlarged by roughly a factor of two in order to insure a smooth pristine glass surface that is free of chemical impurities.
- Cells will be subjected to a long (4–7 day) bake-out at high (¿ 400°$C$) temperature on a high vacuum system before filling.

- Rb will be doubly distilled in such a manner as to avoid introducing any contaminents to the system.
- The $^3$He will be purified either by getters or a liquid $^4$He trap during filling.

The cells will be filled to a high density of $^3$He by maintaining the cell at a temperature of about 20 K during the filling process. This is necessary so that the *pressure* in the cell is below one atmosphere when the glass tube through which the cell is filled is sealed.

The length of the cell has been chosen to be 40 cm so that the end windows will not be within the acceptance of the Hall A spectrometers. The end windows themselves will be about 100 $\mu$ thick. Thinner windows could in principle be used, but this does not appear to be necessary.

### 3.2.3 The Optics System

As mentioned above, approximately 20–24 Watts of "usable" light at 795 nm will be required. By "usable", we mean essentially light that can be readily absorbed by the Rb. It should be noted that the absorption line of the Rb will have a full width of several hundred GHz at the high pressures of $^3$He at which we will operate. Furthermore, since we will operate with very high Rb number densities that are optically quite thick, quite a bit of light that is not well within ther absorption linewidth is still absorbed.

It is our plan to take advantage of new emerging diode laser technology to economically pump the target. Systems are now commercially available in which a single chip produces about 20 watts of light, about half of which is probably usable. Between 2–4 such systems, at a cost of about \$25,000 each, should do the job. There is also a group a Lawrence Livermore Labs that has offered to build us a single chip that can produce 150 watts. While some studies of the use of diode lasers for spin-exchange optical pumping do exist in the literature [31], actual demonstrations of high polarizations in cells suitable for targets are much more recent [32]. It is our opinion that diode lasers will probably work, but we will

perform several tests before freezing this decision.

At SLAC, five titanium-sapphire/argon ion laser systems were used to drive the E-142 polarized $^3$He target. This option will definitely work, but is much more expensive.

### 3.2.4 Polarimetry

Polarimetry will be accomplished by two means. During the experiment, polarization will be monitored using the NMR technique of adiabatic fast passage (AFP) [33]. The signals will be calibrated by comparing the $^3$He NMR signals with those of water. The calibration will be independently verified by studying the frequency shifts that the polarized $^3$He nuclei cause on the electron paramagnetic resonance (EPR) lines of Rb atoms [28]. This second technique will be performed in separate target studies, not during the experiment. It will serve solely as a check of our calibration. We plan to determine the polarization of the target within 5% of itself.

### 3.2.5 Apparatus Overview

The target will be in air, or perhaps, in a helium bag. This greatly simplifies the design. The main components of the target are show in Fig 3. The "main coils" shown are large Helmholtz coils that will be used to apply a static magnetic field of about 20 Gauss. In addition to establishing the quantization axis for the target, the main coils are important for suppressing relaxation due to magnetic field inhinomogeneities, which goes like $1/B^2$. At 20 G, inhomogeneities can be as large as about 30 mG/cm while keeping $\Gamma_{\nabla B}$ ¡ 1/100 hours By increasing the applied field to about 40 G, and relaxing our requirements on $\Gamma_{\nabla B}$ by about factor of two, inhomogeneities as large as 0.25G/cm can be tolerated. We are still finalizing our final choice of static field. The NMR components in the target include a set of RF drive coils, and a separate set of pickup coils. Not shown in the figure are the NMR electronics,which will include an RF power amplifier, a lock-in amplifier, some bridge circuitry, and the capability to sweep the static magnetic field.

The oven shown in Fig. 3 is constructed of Torlon, a high temperature plastic. The oven is heated with forced hot air. The optics system will either inlclude five Ti-sapphire lasers (only one is shown) or 2-4 laser diode system. Either way, there will also be several lenses, and a quarter wave plate to provide the circular polarization.

### 3.3 Spectrometers Systems

We plan to use the Hall A HRS spectrometers as two independent single arm spectrometers in order to optimize the data taking at different angles. The standard detector package configuration of the electron spectrometer shall be used:

- Vertical Drift Chamber's for measurement of momentum and production angle of scattered particles.
- A gas Čerenkov counter for pion rejection.
- A set of scintillators hodoscopes for triggering when combined with the Čerenkov.
- A lead glass calorimeter for additional pion rejection.

For the Hadron spectrometer the standard detector configuration is the same as that of the Electron spectrometer except for the lead glass calorimeter which is replaced by the focal plane polarimeter (FPP). However we will not need additional rejection, since the end windows of the target glass cell are outside the spectrometer acceptance, the rate in the detector is dominated by "good" electrons scattering off the $^3$He gas. This situation is very advantageous compared to our experience in E-142 where the end windows where dominating the rate in the spectrometers. Furthermore due to the excellent target reconstruction in the HRS spectrometers unwanted backgrounds can be analysed and corrected by software.

We shall use the Hadron spectrometer at forward angle where the $\pi/e$ ratio is less then one for a wide range of energy transfer.

# 4. Measurements and Data Analysis

The measurement consists of collecting data at each incident energy and angle for several spectrometers momentum settings to cover the proposed range of kinematics (Tables 1-9). The experimental raw counting asymmetry $\Delta$ shall be converted to the experimental asymmetry $A^{\parallel}$, using the relation

$$\Delta = \frac{(N^{\uparrow\downarrow} - N^{\uparrow\uparrow})}{(N^{\uparrow\downarrow} + N^{\uparrow\uparrow})} \quad , \qquad A^{\parallel} = \frac{\Delta}{P_b P_t f} \quad , \tag{4.1}$$

where $N^{\uparrow\downarrow}$ ($N^{\uparrow\uparrow}$) represents the rate of scattered electrons for each bin of $x$ and $Q^2$ when the electron beam helicity is antiparallel (parallel) to the target spin, and $f$ is the dilution factor that corresponds to the fraction of events that originated from scattering off the neutron in $^3$He. Because no glass is seen by the spectrometer acceptance this factor is close to 0.3. However we will take empty target measurements to insure that no extra dilution of $A^{\parallel}$ occurs from possible background due to end target glass windows. This study will benefit greatly from the excellent target reconstruction by the HRS.

$P_b$ and $P_t$ are the beam and target polarization rspectively. To evaluate the systematic error of the corrected asymmetry we have assumed $\Delta P_b/P_b = 0.03$ and $\Delta P_t/P_t = 0.05$. Uncertainty in $A^{\parallel}$ is dominated by the systematic errors of the target and beam polarizations. We plan to take extra care to minimize these errors. An elastic scattering asymmetry measurement is planned at small energies in order to measure the product of the target density by the polarization. This quantity can be evaluated using the measured electric and magnetic form factors of $^3He$. This measurement would be unique as to determine the polarization of the $^3$He nuclei along the electron beam path.

Also contributing to the dilution of the asymmetry is the pair-electron contamination which will be measured by reversing the spectrometer polarity. This correction is $x$ dependent, and dominate in the low $x$ region. False asymmetries shall be verified to be consistent with zero by comparing data with target spins in opposite directions.

External radiative corrections will be evaluated and applied using the Mo and Tsai method [35], because of the relatively thin target ($\sim$ 0.3% radiation length) external corrections are very small. Internal radiative corrections are more important, and shall be evaluated using the exact procedure of Kukhto and Shumeiko [34]. A first estimate of the total radiative corrections amounted to a relative change in the asymmetry ranging from 10% at low $x$ to 15% at large $x$. More studies are underway to properly treat the resonance region. The corrections in the $\Delta$ region will depend on the quasielastic tails asymmetries.

Recent studies by several groups [36,37,38] have concluded that in deep-inelastic scattering a polarized $^3$He nucleus target can be regarded as a good model of a polarized neutron, provided a small correction for the $S'$ and $D$ states is applied. To extract the neutron asymmetry from the measured $^3$He asymmetry, we shall follow the method described in [37], allowing for a correction from the polarization of the two protons in $^3$He ($\sim -2.7\%$ per proton) and a correction for the polarization of the neutron in $^3$He ($\sim$87%).

To estimate the rates presented in Table 1 to 9, we assumed an electron beam current of $15\mu A$, the standard angular ($\Delta\Omega$ = 7.3 msr) and HRS momentum acceptance ($\delta p/p = \pm 0.05$). Combined with our target density the luminosity is close to $10^{36}$. We took $\Delta A$ = 0.5% for the absolute statistical error on the asymmetry measurement for each spectrometer momentum bin to define the time estimate.

As can be seen in the rate tables, the cross sections at forward angle and small incident beam energies are quite large. We will tune the current intensity to keep the data aquisition running smoothly. The spin dependent cross sections were evaluated using a resonance model developed by Burkert and Li, while above W$^2$ = 4 GeV$^2$ a parametrization of the E-142 measured asymmetry was used.

Figure 4 shows the expected results on the $Q^2$ dependence of the extended Drell-Hearn-Gerasimov for the neutron. The curves shown are from the program AO ( based on an analysis of eletromagnetic transition amplitudes in the resonance region) [40], with different

assumptions on the structure of the Roper resonance). The Chiral perturbation theory [13] prediction is also reported along with the $Q^2 = 0$ predicted values for DHG and the pion photoproduction data by Workman et al. [18]

## 5. Summary and Request

We propose to measure the spin structure function of the neutron ($^3$He) across the resonance and inelastic region. These data allow the investigation of the extended Drell-Hearn-Gerassimov from $Q^2 = 0.15$ GeV$^2$ to $Q^2 = 2.$ GeV$^2$.

The beam time requested is 650 hours. This includes 500 hours for the longitudinal asymmetry measurements, and 100 hours devoted to the transverse asymmetry measurement to reduce the systematic error due to $A_2$ and pair-electron measurements in the low x region. An overhead for energy, angles and spectrometer momentum changes of 50 hours is considered. Four days for setup are

In summary, a total of 31 days of running is requested.

# REFERENCES


[1] EM Collab., J. Ashman *et al.*, Phys. Lett **B 206**(1988)364; Nucl. Phys. **B 328** (1989)1

[2] SLAC-E142. P.L. Anthony, *et al.*, Phys. Rev. Lett. **71** (1993)959

[3] SM Collab., B. Adeva *et al.*, Phys. Lett. **B 302** (1993) 533

[4] Larin, S.A., Vermaseren, J.A.M.: Phys . Lett. **B259**, 345 (1991)

[5] E. Shuryak and A. Vainshtein, Nucl. Phys. **B199** (1982)451; Nucl.Phys. **B201**(1982) 141

[6] V. Bernard, N. Kaiser, Ulf-G. Meissner, Phys. Rev. **D48** (1993)

[7] Balitsky, I.I., Braun, V.M., Kolesnichenko, A.V.: Phys. Lett. **B242**, 145 (1990); Errata, Phys. Lett. **B318** (1993)648-650

[8] X. Ji and M. Unrau preprint MIT-CTP-2232 (August 1993)

[9] G. G. Ross and R.G. Roberts Phys. Lett. **B 322** (1994)

[10] S. D. Drell and A.C. Harn, Phys. Rev. Lett. **16** (1966)908; S. B. Gerasimov, Sov. J. Nucl. Phys. **2**(1966)430.

[11] M. Anselmino, B. L. Ioffe, and E. Leader, Sov. J. Nucl. Phys. 49(1989) 553

[12] Z.P. Li, V. Burkert and Z. Li, Phys. Rev. D **46**, (1992)70

[13] V. Bernard, N. Kaiser and U.-G. Meissner, Phys. Rev. **D48** (1993)3062

[14] J. Soffer and O. Teryaev Phys. Rev. Lett. **70** (1993)3373

[15] C.E. Carlson and W.-K. Tung, Phys. Rev. **D5**(1972)721.

[16] A.J.G. Hey and J.E. Mandula, Phys. Rev. **D5**(1972)2610.

[17] I. Karliner, Phys. Rev. **D7**(1973)2717.

[18] R. L. Workman and R. A. Arndt, Phys. Rev. **45** (1992)1789.

[19] V. Burkert and Z. Li, Phys. Rev. **D47** (1993)46.

[20] L.S. Cardman and C.K. Sinclair, CEBAF memo (1993)

[21] T.E. Chupp, M.E. Wagshul, K.P. Coulter, A.B. McDonald, and W. Happer, Phys. Rev. C **36** (1987)2244.

[22] W. Happer, Rev. Mod. Phys. **44**(1972)169.

[23] M.A. Bouchiat, T.R. Carver and C.M. Varnum, Phys. Rev. Lett. **5** (1960)373.

[24] N.D. Bhaskar, W. Happer, and T. McClelland, Phys. Rev. Lett. **49** (1982)25.

[25] W. Happer, E. Miron, S. Schaefer, D. Schreiber, W.A. van Wijngaarden, and X. Zeng, Phys. Rev. A **29**(1984)3092.

[26] K.P. Coulter, A.B. McDonald, W. Happer, T. E. Chupp, and M.E. Wagshul, Nuc. Inst. Meth. in Phys. Res. **A 270** (1988)90.

[27] N.R. Newbury, A.S. Barton, P. Bogorad, G. D. Cates, M. Gatzke, H. Mabuchi, and B. Saam, Phys. Rev. A **48** (1993)558.

[28] N. R. Newbury, A. S. Barton, G. D. Cates, W. Happer, and H. Middleton, Phys. Rev. A **48** (1993)4411.

[29] G.D. Cates, S.R. Schaefer and W. Happer, Phys. Rev. A **37**, 2877 (1988); G.D. Cates, D.J. White, Ting-Ray Chien, S.R. Schaefer and W. Happer, Phys. Rev. A **38** (1988)5092.

[30] K.P. Coulter, A.B. McDonald, G.D. Cates, W. Happer, T.E. Chupp, Nuc. Inst. Meth. in Phys. Res. **A276** (1989)29.

[31] M.E. Wagshul, T.E. Chupp, Phys. Rev **A 40** (1989)4447.

[32] B. Cummings, Private communication

[33] A. Abragam, Principles of Nuclear Magnetism (Oxford University Press, New York, 1961).

[34] T.V. Kukhto and N.M. Shumeiko, Nucl. Phys. **219** (1983)412.

[35] L.W. Mo and Y.T. Tsai, Rev. Mod. Phys. **41** (1969)205.

[36] B. Blankleider and R.M. Woloshyn, Phys. Rev. C **29** (1984)538.

[37] C. Ciofi degli Atti, S. Scopetta, E. Pace, G. Salme, University of Perugia report N0. DFUPG-75/93 (to be published) and see G. Salme in these Proceedings

[38] R.-W. Shulze and P.U. Sauer, Phys. Rev. C**48** (1993)38.

[39] V. Burkert and Z. Li, Phys. Rev. D**47**, 46

[40] S. Kuhn, Private communication and Proposal E-93-009.

| Table 1 | | | $E_i = 4GeV$ $\theta = 15°$ | | | | |
|---|---|---|---|---|---|---|---|
| $e'$ (GeV) | $\nu$ (GeV) | $x$ | $Q^2$ (GeV/c)$^2$ | $D$ | $A_{\|\|}$ | Rate (Hz) | Time (hrs) |
| 3.30 | 0.70 | 0.685 | 0.90 | 0.174 | -0.005 | 1027.46 | 0.34 |
| 2.90 | 1.10 | 0.383 | 0.79 | 0.267 | -0.028 | 2259.32 | 0.19 |
| 2.70 | 1.30 | 0.302 | 0.74 | 0.316 | -0.024 | 2044.34 | 0.20 |
| 2.50 | 1.50 | 0.242 | 0.68 | 0.368 | -0.008 | 2024.97 | 0.22 |
| 2.30 | 1.70 | 0.197 | 0.63 | 0.423 | -0.030 | 1607.87 | 0.25 |
| 2.00 | 2.00 | 0.145 | 0.55 | 0.510 | -0.037 | 1257.42 | 0.33 |
| 1.80 | 2.20 | 0.119 | 0.49 | 0.570 | -0.037 | 1050.65 | 0.39 |
| 1.60 | 2.40 | 0.097 | 0.44 | 0.631 | -0.055 | 873.26 | 0.47 |
| 1.40 | 2.60 | 0.078 | 0.38 | 0.693 | -0.057 | 720.88 | 0.56 |
| 1.20 | 2.80 | 0.062 | 0.33 | 0.753 | -0.058 | 589.29 | 0.68 |
| 1.00 | 3.00 | 0.048 | 0.27 | 0.806 | -0.057 | 474.19 | 0.84 |
| 0.70 | 3.30 | 0.031 | 0.19 | 0.855 | -0.054 | 323.46 | 1.23 |
| | | | | | | | Total = 5hrs |

Table 2 $E_i = 4GeV \quad \theta = 25°$

| $e'$ (GeV) | $\nu$ (GeV) | $x$ | $Q^2$ (GeV/c)$^2$ | $D$ | $A_\parallel$ | Rate (Hz) | Time (hrs) |
|---|---|---|---|---|---|---|---|
| 2.70 | 1.30 | 0.830 | 2.02 | 0.363 | 0.001 | 26.69 | 13.42 |
| 2.50 | 1.50 | 0.666 | 1.87 | 0.412 | -0.002 | 71.70 | 5.89 |
| 2.30 | 1.70 | 0.540 | 1.72 | 0.460 | -0.027 | 130.56 | 3.71 |
| 2.10 | 1.90 | 0.441 | 1.57 | 0.509 | -0.027 | 152.03 | 3.15 |
| 1.90 | 2.10 | 0.361 | 1.42 | 0.558 | -0.066 | 137.21 | 3.07 |
| 1.70 | 2.30 | 0.295 | 1.27 | 0.607 | -0.073 | 137.00 | 3.11 |
| 1.50 | 2.50 | 0.240 | 1.12 | 0.657 | -0.069 | 127.90 | 3.30 |
| 1.30 | 2.70 | 0.192 | 0.97 | 0.709 | -0.084 | 115.76 | 3.61 |
| 1.00 | 3.00 | 0.133 | 0.75 | 0.789 | -0.081 | 94.84 | 4.34 |
| 0.80 | 3.20 | 0.100 | 0.60 | 0.843 | -0.089 | 80.19 | 5.09 |
| | | | | | | | Total = 50hrs |

Table 3 $E_i = 4.GeV \quad \theta = 35°$

| $e'$ (GeV) | $\nu$ (GeV) | $x$ | $Q^2$ (GeV/c)$^2$ | $D$ | $A_\parallel$ | Rate (Hz) | Time (hrs) |
|---|---|---|---|---|---|---|---|
| 2.10 | 1.90 | 0.852 | 3.04 | 0.569 | -0.032 | 4.32 | 109.24 |
| 1.90 | 2.10 | 0.698 | 2.75 | 0.616 | 0.001 | 9.57 | 46.39 |
| 1.70 | 2.30 | 0.570 | 2.46 | 0.661 | -0.018 | 17.32 | 26.06 |
| 1.50 | 2.50 | 0.463 | 2.17 | 0.704 | -0.094 | 21.76 | 19.87 |
| 1.30 | 2.70 | 0.371 | 1.88 | 0.746 | -0.103 | 25.22 | 17.25 |
| 1.10 | 2.90 | 0.292 | 1.59 | 0.786 | -0.096 | 26.15 | 16.43 |
| 0.90 | 3.10 | 0.224 | 1.30 | 0.827 | -0.105 | 25.30 | 16.73 |
| 0.70 | 3.30 | 0.164 | 1.01 | 0.869 | -0.114 | 23.07 | 18.04 |
| 0.60 | 3.40 | 0.136 | 0.87 | 0.891 | -0.108 | 21.53 | 19.17 |
| | | | | | | | Total = 289 hrs |

Table 4 $E_i = 3.2GeV \quad \theta = 15°$

| $e'$ (GeV) | $\nu$ (GeV) | $x$ | $Q^2$ (GeV/c)$^2$ | $D$ | $A_\parallel$ | Rate (Hz) | Time (hrs) |
|---|---|---|---|---|---|---|---|
| 2.60 | 0.60 | 0.504 | 0.57 | 0.188 | -0.043 | 6103.35 | 0.08 |
| 2.40 | 0.80 | 0.349 | 0.52 | 0.248 | -0.037 | 3182.98 | 0.12 |
| 2.20 | 1.00 | 0.256 | 0.48 | 0.313 | -0.046 | 4145.17 | 0.12 |
| 2.00 | 1.20 | 0.194 | 0.44 | 0.381 | -0.022 | 2904.57 | 0.15 |
| 1.80 | 1.40 | 0.149 | 0.39 | 0.454 | -0.018 | 2201.78 | 0.18 |
| 1.50 | 1.70 | 0.103 | 0.33 | 0.564 | -0.039 | 1533.10 | 0.26 |
| 1.20 | 2.00 | 0.070 | 0.26 | 0.669 | -0.041 | 1038.11 | 0.39 |
| 0.90 | 2.30 | 0.045 | 0.20 | 0.747 | -0.058 | 685.40 | 0.58 |
| 0.60 | 2.60 | 0.027 | 0.13 | 0.769 | -0.055 | 417.75 | 0.95 |
| | | | | | | | Total = 3hrs |

Table 5 $E_i = 3.2GeV \quad \theta = 25°$

| $e'$ (GeV) | $\nu$ (GeV) | $x$ | $Q^2$ (GeV/c)$^2$ | $D$ | $A_\parallel$ | Rate (Hz) | Time (hrs) |
|---|---|---|---|---|---|---|---|
| 2.20 | 1.00 | 0.703 | 1.32 | 0.341 | -0.063 | 225.40 | 2.27 |
| 2.10 | 1.10 | 0.610 | 1.26 | 0.371 | -0.059 | 194.32 | 2.21 |
| 1.90 | 1.30 | 0.467 | 1.14 | 0.431 | -0.044 | 261.26 | 1.69 |
| 1.70 | 1.50 | 0.362 | 1.02 | 0.493 | -0.043 | 248.99 | 1.68 |
| 1.50 | 1.70 | 0.282 | 0.90 | 0.557 | -0.051 | 234.01 | 1.75 |
| 1.30 | 1.90 | 0.219 | 0.78 | 0.624 | -0.073 | 212.64 | 1.96 |
| 1.10 | 2.10 | 0.167 | 0.66 | 0.695 | -0.073 | 180.59 | 2.28 |
| 0.90 | 2.30 | 0.125 | 0.54 | 0.766 | -0.071 | 148.79 | 2.75 |
| 0.70 | 2.50 | 0.089 | 0.42 | 0.838 | -0.090 | 118.01 | 3.44 |
| | | | | | | | Total = 20 hrs |

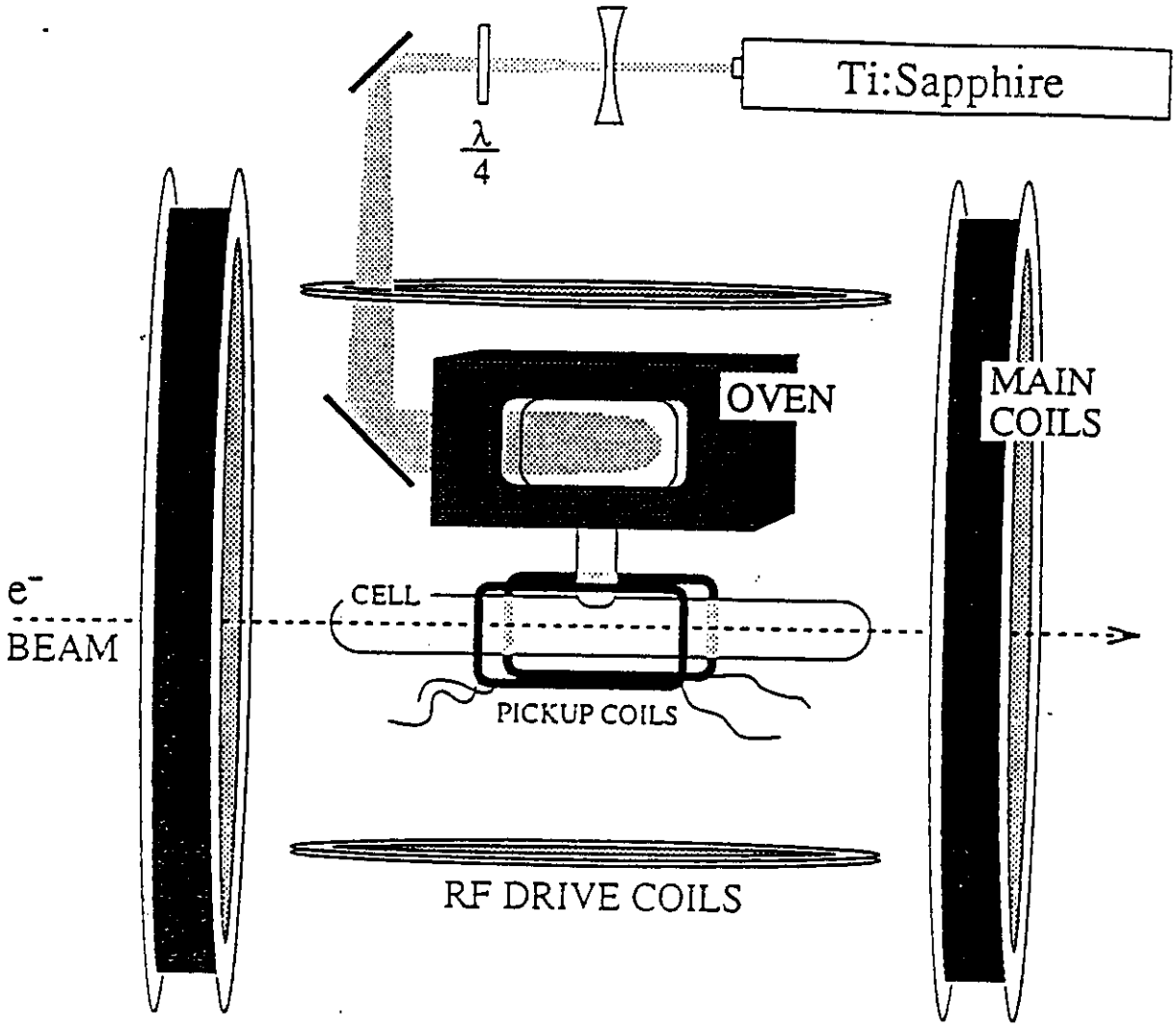


Shown is a schematic representation of the SLAC E-142 polarized $^3$He target. Only one of the five titanium-sapphire/argon ion laser systems are shown. Not shown are the transverse coils and the window cooling system.

Fig 3

# DHG Sum Rule for the Neutron

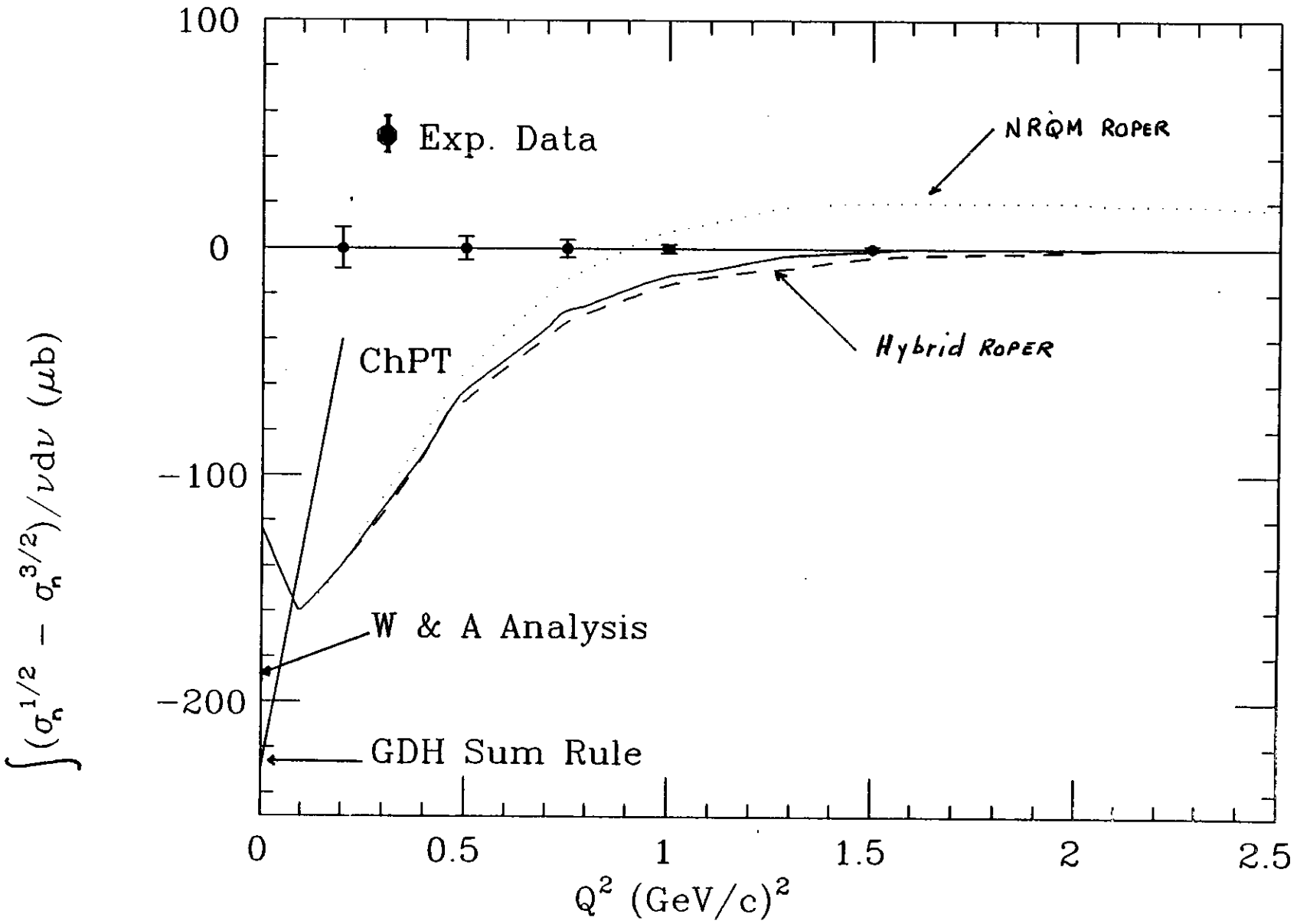


Fig 4

| Table 6 | | | $E_i = 3.2GeV$ $\theta = 35°$ | | | | |
|---|---|---|---|---|---|---|---|
| $e'$ (GeV) | $\nu$ (GeV) | $x$ | $Q^2$ (GeV/c)$^2$ | $D$ | $A_\parallel$ | Rate (Hz) | Time (hrs) |
| 1.80 | 1.40 | 0.793 | 2.08 | 0.517 | -0.050 | 18.09 | 27.52 |
| 1.60 | 1.60 | 0.617 | 1.85 | 0.574 | -0.013 | 24.76 | 17.56 |
| 1.40 | 1.80 | 0.480 | 1.62 | 0.631 | -0.058 | 38.01 | 11.02 |
| 1.20 | 2.00 | 0.370 | 1.39 | 0.687 | -0.091 | 43.60 | 9.56 |
| 1.00 | 2.20 | 0.280 | 1.16 | 0.743 | -0.110 | 44.97 | 9.43 |
| 0.80 | 2.40 | 0.206 | 0.93 | 0.801 | -0.106 | 41.15 | 10.16 |
| 0.60 | 2.60 | 0.142 | 0.69 | 0.862 | -0.105 | 35.12 | 11.74 |
| | | | | | | | Total = 97 hrs |

| Table 7 | | | $E_i = 2.4GeV$ $\theta = 15°$ | | | | |
|---|---|---|---|---|---|---|---|
| $e'$ (GeV) | $\nu$ (GeV) | $x$ | $Q^2$ (GeV/c)$^2$ | $D$ | $A_\parallel$ | Rate (Hz) | Time (hrs) |
| 2.00 | 0.40 | 0.436 | 0.33 | 0.176 | -0.020 | 4226.15 | 0.08 |
| 1.80 | 0.60 | 0.261 | 0.29 | 0.258 | -0.060 | 6314.82 | 0.06 |
| 1.50 | 0.90 | 0.145 | 0.25 | 0.387 | -0.068 | 4870.53 | 0.09 |
| 1.30 | 1.10 | 0.103 | 0.21 | 0.467 | -0.029 | 3264.06 | 0.14 |
| 1.10 | 1.30 | 0.074 | 0.18 | 0.534 | -0.027 | 1998.66 | 0.20 |
| 0.90 | 1.50 | 0.052 | 0.15 | 0.581 | -0.042 | 1381.44 | 0.29 |
| 0.70 | 1.70 | 0.036 | 0.11 | 0.602 | -0.046 | 920.63 | 0.43 |
| 0.60 | 1.80 | 0.029 | 0.10 | 0.601 | -0.045 | 736.52 | 0.54 |
| | | | | | | | Total = 2 hrs |

Table 8 $E_i = 2.4GeV \quad \theta = 25°$

| $e'$ (GeV) | $\nu$ (GeV) | $x$ | $Q^2$ (GeV/c)$^2$ | $D$ | $A_\parallel$ | Rate (Hz) | Time (hrs) |
|---|---|---|---|---|---|---|---|
| 1.70 | 0.70 | 0.582 | 0.76 | 0.319 | -0.074 | 680.35 | 0.74 |
| 1.50 | 0.90 | 0.399 | 0.67 | 0.400 | -0.066 | 422.14 | 0.95 |
| 1.30 | 1.10 | 0.283 | 0.58 | 0.488 | -0.082 | 534.26 | 0.85 |
| 1.10 | 1.30 | 0.203 | 0.49 | 0.582 | -0.040 | 460.08 | 0.99 |
| 0.90 | 1.50 | 0.144 | 0.40 | 0.681 | -0.062 | 305.40 | 1.31 |
| 0.70 | 1.70 | 0.099 | 0.31 | 0.776 | -0.076 | 229.92 | 1.76 |
| 0.60 | 1.80 | 0.080 | 0.27 | 0.816 | -0.075 | 192.18 | 2.09 |
| | | | | | | | Total= 10 hrs |

Table 9 $E_i = 1.6GeV \quad \theta = 15°$

| $e'$ (GeV) | $\nu$ (GeV) | $x$ | $Q^2$ (GeV/c)$^2$ | $D$ | $A_\parallel$ | Rate (Hz) | Time (hrs) |
|---|---|---|---|---|---|---|---|
| 1.30 | 0.30 | 0.252 | 0.14 | 0.157 | -0.022 | 7610.70 | 0.05 |
| 1.20 | 0.40 | 0.174 | 0.13 | 0.197 | -0.070 | 18860.97 | 0.02 |
| 1.10 | 0.50 | 0.128 | 0.12 | 0.232 | -0.072 | 8418.18 | 0.05 |
| 1.00 | 0.60 | 0.097 | 0.11 | 0.263 | -0.064 | 5470.71 | 0.07 |
| 0.90 | 0.70 | 0.075 | 0.10 | 0.289 | -0.061 | 4495.44 | 0.09 |
| 0.80 | 0.80 | 0.058 | 0.09 | 0.310 | -0.087 | 4224.84 | 0.11 |
| 0.70 | 0.90 | 0.045 | 0.08 | 0.324 | -0.073 | 2648.07 | 0.15 |
| 0.60 | 1.00 | 0.035 | 0.07 | 0.332 | -0.042 | 2139.98 | 0.21 |
| | | | | | | | Total= 1 hour |

## Figure Captions

Figure 1.

A summary of the experimental investigation of the nucleon spin spin structure function. World results and test of the Bjorken sum rule at $Q^2 \geq 1$ GeV$^2$

Figure 2.

a) Kinematical range ($Q^2, \nu$ ) covered by the proposed measurement along with the range measured in E-142 at SLAC. b) Same as a) but for ($Q^2$,x), where x is the Bjorken Variable

Figure 3 A schematic representation of the SLAC E-142 polarized $^3$He target. Not shown are the transverse coils and the window cooling system.

Figure 4.

Expected results on the $Q^2$ dependence of the extended Drell-Hearn-Gerasimov for the neutron. The curves shown are from the program AO ( based on an analysis of eletromagnetic transition amplitudes in the resonance region) [40], with different assumptions on the structure of the Roper resonance). The Chiral perturbation theory [13] prediction is also reported along with the $Q^2 = 0$ predicted values for DHG and the pion photoproduction data by Workman et al. [18]

Fig 1.

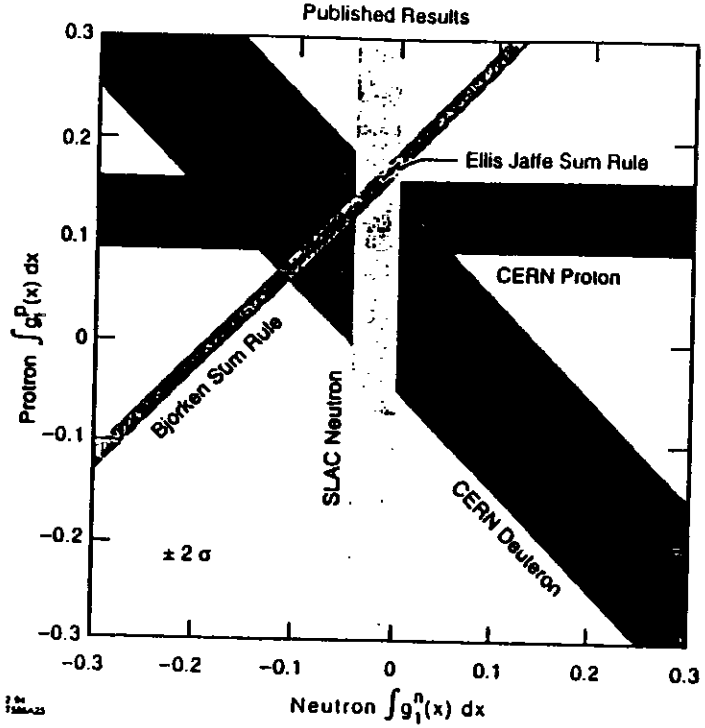


Results on the integrals $\int g_1^p$ versus $\int g_1^n$ from CERN and SLAC compared to the Bjorken (a line) and the Ellis-Jaffe (a point) sum rules. Bands correspond to $\pm 2\sigma$.

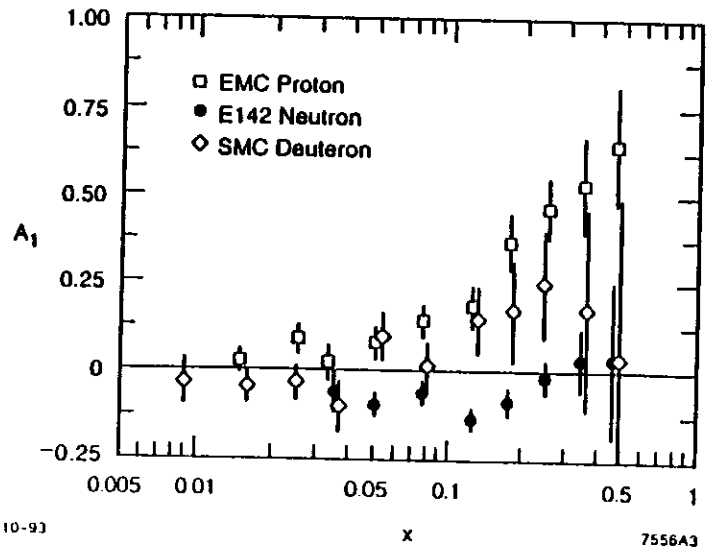


Comparison of $A_1$ verus $x$ of the CERN EMC pro
the SLAC E-142 neutron, and the CERN SMC deuteron

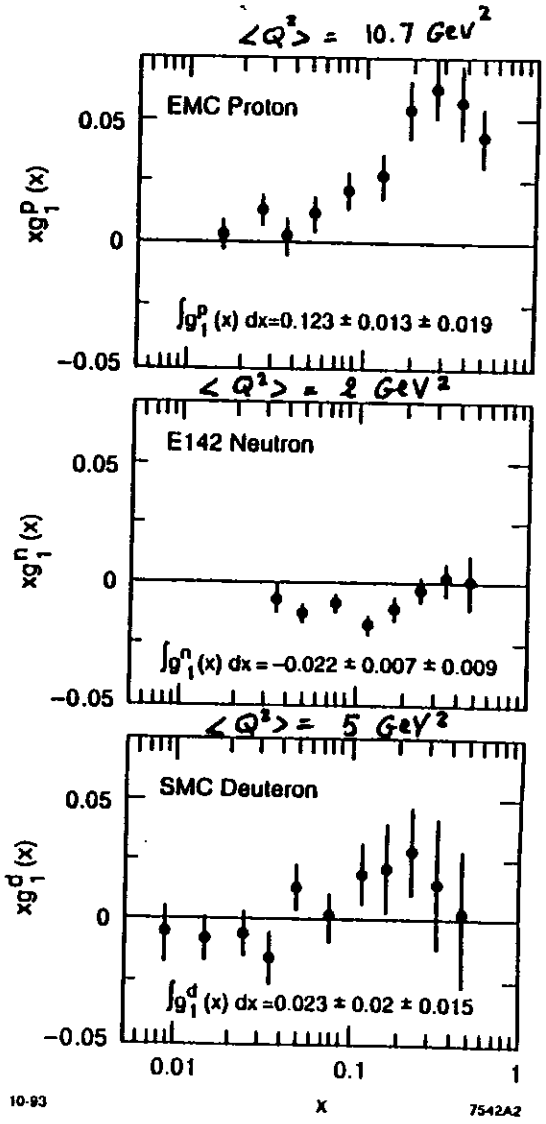


Comparison of $xg_1$ versus $x$ for the CERN EMC proton, E-142 neutron, and the CERN SMC deuteron. Here the deuteron by convention as being the average of

SLAC
efined

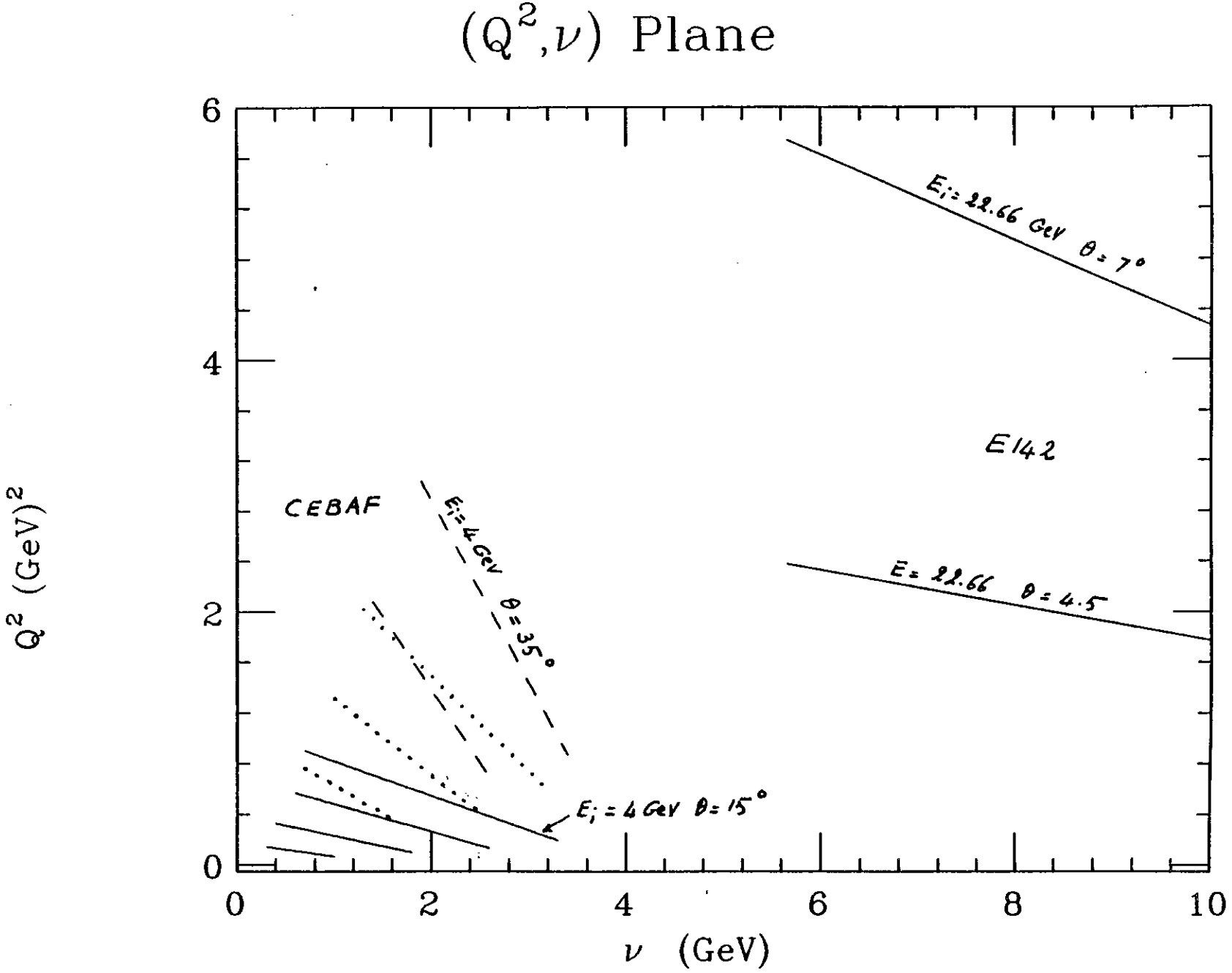
$(Q^2,\nu)$ Plane
$Q^2$ (GeV)$^2$
$\nu$ (GeV)
0
2
4
6
8
10
CEBAF
E142
$E_i$ = 4 GeV θ = 35°
$E_i$ = 4 GeV θ = 15°
$E_i$ = 22.66 GeV θ = 7°
E = 22.66 θ = 4.5

Fig 2a

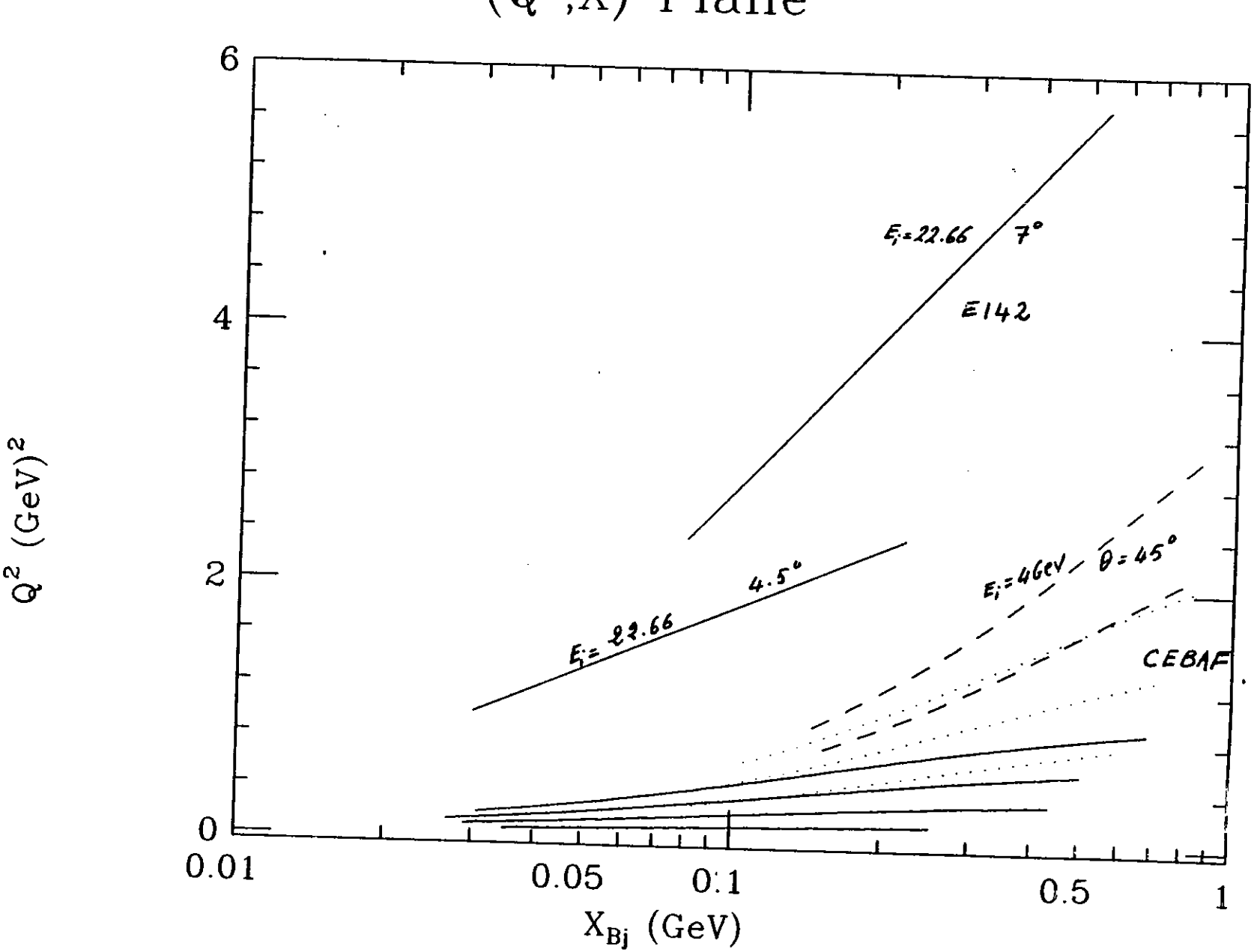
(Q²,X) Plane
6
4
2
0
0.01
0.05
0.1
0.5
1
Q² (GeV)²
X_Bj (GeV)
E_i=22.66 7°
E142
E_i=22.66 4.5°
E_i=46eV θ=45°
CEBAF

Fig 2b

# HAZARD IDENTIFICATION CHECKLIST

CEBAF Experiment: PR-94-10 Date: June 09 94

Check all items for which there is an anticipated need—do not check items that are part of the CEBAF standard experiment (HRSE, HRSH, CLAS, HMS, SOS in standard configurations).

**Cryogenics**
- ____ beamline magnets
- ____ analysis magnets
- ____ target
- ____ drift chambers
- ____ other

**Electrical Equipment**
- ____ cryo/electrical devices
- ____ capacitor banks
- ____ high voltage
- ____ exposed equipment

**Radioactive/Hazardous Materials**
List any radioactive or hazadorous/toxic materials planned for use:
____
____

**Pressure Vessels**
- 4 cm inside diameter
- 12 atm operating pressure
- Glass window material
- 100 μm window thickness

Glass cells must be treated as having potential to burst

**Flammable Gas or Liquids**
(incl. target)
- type: ____
- flow rate: ____
- capacity: ____

**Other Target Materials**
- ___ Beryllium (Be)
- ___ Lithium (Li)
- ___ Mercury (Hg)
- ___ Lead (Pb)
- ___ Tungsten (W)
- ___ Uranium (U)
- ___ Other (list below)

____
____

**Vacuum Vessels**
- ____ inside diameter
- ____ operating pressure
- ____ window material
- ____ window thickness

**Radioactive Sources**
- ____ permanent installation
- ____ temporary use
- type: ____
- strength: ____

**Large Mech. Structure/System**
- ____ lifting devices
- ____ motion controllers
- ____ scaffolding or elevated platforms
- ____ other

**Lasers** Diode / $Ar^+$
- type: Ti:sapphire
- wattage: 20 - 40 W
- class: IV

**Installation**
- ____ permanent
- x temporary

**Use**
- ____ calibration
- ____ alignment

Polarized target. ($^3He$)

**Hazardous Materials**
- ____ cyanide plating materials
- ____ scintillation oil (from)
- ____ PCBs
- ____ methane
- ____ TMAE
- ____ TEA
- ____ photographic developers
- ____ other (list below)

____
____
____

**Notes:**
____
____
____
____
____
____